Electronic Supplementary Material (ESI) for Analyst.

Supporting Information for:

The Role of Solvation on the Conformational Landscape of α-Synuclein.

Melanie Cheung See Kit,[1] Tyler C. Cropley,[2] Christian Bleiholder,[2,3] Christopher D. Chouinard,[4] Frank Sobott,[5] Ian K. Webb[1,6*]

[1]Department of Chemistry and Chemical Biology, Indiana University-Purdue University Indianapolis, Indianapolis, Indiana 46202, United States

[2]Department of Chemistry and Biochemistry, Florida State University, Tallahassee, Florida 32306, United States

[3]Institute of Molecular Biophysics, Florida State University, Tallahassee, Florida 32306, United States

[4]Department of Chemistry, Clemson University, Clemson, South Carolina 29625, United States

[5]Astbury Centre for Structural Molecular Biology, School of Molecular and Cellular Biology, Faculty of Biological Sciences, University of Leeds, Leeds LS2 9JT, United Kingdom

[6]Center for Computational Biology and Bioinformatics, Indiana University School of Medicine, Indianapolis, Indiana 46202, United States

*To whom correspondence should be addressed; e-mail: ikwebb@iu.edu

Table of Contents

Supporting Methods.

Materials. Ammonium acetate, triethyl ammonium bicarbonate (TEAB) ubiquitin from bovine erythrocytes, myoglobin from horse heart, cytochrome c from equine heart, potassium benzene-1,2-disulfonate (1,2-BDSA), 1,3-benzenedisulfonic acid disodium salt (1,3-BDSA), 1,5-napthalenedisulfonic acid, disodium salt hydrate (1,5-NDSA), and pentadecafluoro-1-octanol (PFO) were purchased from Sigma-Aldrich (St. Louis, MO). Ethylene glycol bis(sulfosuccinimidyl succinate) (Sulfo-EGS), bis(sulfosuccinimidyl)suberate (BS3), bis(sulfosuccinimidyl) glutarate-d0 (BS2G) disodium forms, 1-ethyl-3-(3-dimethylaminopropyl)carbodiimide hydrochloride (EDC), 3-morpholinopropane-1-sulfonic acid (MOPS), and Zeba spin desalting columns 7K MWCO and Amberlite IR-120 (H) ion-exchange resin were obtained from ThermoFisher Scientific (Rockford, IL). Methanol, acetonitrile, ammonium hydroxide, malonic acid dihydrazide (MDH), and phosphate-buffered saline components (1X PBS: 137 mM NaCl, 2.7 mM KCl, 10 mM Na2HPO4 and 2 mM KH2PO4) were purchased from Fisher Scientific (Fairmont, NJ). 3-hydroxytriazolo[4,5-b]pyridine (HOAt) was purchased from ApexBio Technology (Boston, MA). Glu-C (sequencing grade) was purchased from Promega (Madison, WI, USA) and water was obtained from a Milli-Q Millipore A10 (Burlington, MA) water purification system at a resistivity of 18 MΩ or greater. **Protein Expression, Purification and In-Solution Crosslinking.** The plasmid pET21a-alpha-synuclein was a gift from Michael J Fox Foundation MJFF (Addgene plasmid # 51486, Watertown, MA, USA). The untagged human protein was expressed in *E. coli* BL21 cells and purified following a previously published protocol.[1] Prior to crosslinking reactions, αSN aliquots were buffer exchanged into 1X PBS, pH 7.4 using Zeba spin columns. For crosslinking with the amine reactive reagents BS2G (7.7 Å), BS3 (11.4 Å), and sulfo-EGS (16.1 Å), the protein was incubated for 15 minutes at room temperature with 2.5-fold excess crosslinking reagent in 1X PBS at final concentrations of 50 μM and 125 μM respectively. For acidic residue crosslinking, the same final concentration of αSN was reacted with 400-fold excess HOAt (20 mM), 1600-fold excess EDC (80 mM) and 1280-fold excess MDH (8.5 Å) or ADH (11.1 Å)[2] in 50 mM MOPS buffer, pH 6.85,

for 22 minutes at room temperature. The increased molar excess for acidic crosslinking is due to the relatively slow reaction rate near pH 7[3] compared to the amine-reactive crosslinks. The reaction mixture was then buffer exchanged twice into 50 mM ammonium acetate, pH 6.85 to quench the reaction, remove excess crosslinker and transfer the crosslinked samples into a more suitable solution for MS analysis. For the bottom-up experiments with BS2G, BS3, and sulfo-EGS the crosslinked protein (50 μM) was diluted to 10 μM (~0.15 μg/μL) in 50 μL of 50 mM TEAB, pH 8.5 and digested with 0.1 μg Glu-C (~75:1 protein:Glu-C by mass) at 37°C for 18 hours. Since αSN does not contain any cysteine residues, protein reduction and alkylation steps were omitted.

Ion Mobility Mass Spectrometry and CCS Measurements. Drift Tube Ion Mobility Instrument: Drift tube ion mobility spectrometry (DTIMS) measurements were performed using an Agilent Technologies (Santa Clara, CA) 6560 IM-QTOF instrument. Samples were direct infused via syringe pump at 10 μL/min into an Agilent Jet Stream (AJS) dual ESI source. CCS measurements were made using the step-field method with five electric field values of 18.5, 17.3, 16.0, 14.7, and 13.4 V/cm in Agilent MassHunter IM-MS Browser 10.0.1. All other experimental conditions can be found in the table below. The conditions were optimized for native collision cross section (CCS) and conformational profile for native ubiquitin, as in agreement with other published values obtained for the compact conformation of the native state. The drift tube was maintained at approx. 4 Torr nitrogen gas under ambient temperature (~27 °C). The drift tube was operated with a field strength of 19.1 V/cm. CCS were calculated using the single-field method, which involves measurement of the CCS for Agilent Tune Mix ions (m/z 322-2721) to determine both β and T-Fix values. All IM-MS data was visualized and processed using Agilent IM-Browser 10.0. Table S1 outlines the instrument tuning parameters used.

Traveling Wave Ion Mobility Spectrometry: Calibration of drift time measurements to known collision cross section values is necessary for traveling wave ion mobility spectrometry (TWIMS) instruments that use time-varying electric fields within the drift region. Traveling-wave drift times were calibrated by measuring TWIMS profiles of a calibrant mix for each set of experiments

following a previously published protocol. The calibrant mix used for CCS calculations consisted of 1 μM ubiquitin, cytochrome C, and myoglobin in 50:50:0.1 (v/v) solution of methanol/water/formic acid and the instrument settings are listed in Table S2. A calibration curve was obtained by plotting natural logarithm of the nitrogen CCS to charge ratios versus the calibrant ion drift times.[4] The data was fit with a power function of the form, where CCS N_2 is the calibrant nitrogen CCS value, z is the charge state of the ion, and td is the drift time.

Ion/ion Reactions and Tandem Mass Spectrometry. Native top-down experiments were performed on a modified Synapt G2-Si mass spectrometer (Waters Corporation, Wilmslow, UK), equipped with an electron transfer dissociation (ETD) glow discharge source, an external electrospray voltage control module (GAA Custom Electronics LLC, Kennewick, WA, USA) and an ExD cell (e-MSion, Corvallis, OR, USA). Instrumental details for the gas phase ion/ion reactions[5-6] and electron capture dissociation (ECD) using the electromagnetostatic (EMS) cell[7] have been previously described. Protein (50 μM) was electrosprayed in positive ion mode (+0.95 kV) using the NanoLockspray source via borosilicate tips pulled using a P-97 micropipette puller (Sutter Instruments, Novato, CA, USA). Individual charge states of αSN and its crosslinked products (1XL products) were mass-selected in the quadrupole and analyzed by ion mobility (IM) using nitrogen as the mobility gas at a flowrate of 20 mL/min while the Trap and Helium cell flowrates were set to 1 and 200 mL/min respectively. The wave velocity and wave height in the trap, mobility and transfer cells were set as follows: 300 m/s and 5 V, 800 m/s and 20 V and 169 m/s and 5 V respectively. To localize crosslinked sites, isolated species were fragmented by electron capture dissociation (ECD, 3.5 eV electrons) in the EMS cell and analyzed in a 50 – 5,000 m/z window using the time-of-flight (TOF) mass spectrometer in 'Resolution' mode.

Glu-C digested peptides were analyzed by nano-LC-MS/MS using an Ultimate 3000 RSLC nano-HPLC system (Thermo Fisher Scientific, Sunnyvale, CA, USA) coupled to a Thermo Q Exactive orbitrap mass spectrometer equipped with a Nanospray Flex ion source (Thermo Fisher Scientific, Bremen, Germany). Peptides were first trapped on a C18 precolumn (Acclaim PepMap

100, 100 µm x 2 cm, 5 µm, 100 Å, Thermo Fisher Scientific, Sunnyvale, CA, USA) and separated on a C18 column (1.7 µm C18 (100 Å), 75 µm ID x 20 cm L x 365 µm OD; CoAnn Technologies, Richland, WA, USA) over 90 mins by linearly ramping the %ACN from 4% (v/v) to 40% (v/v) at constant pH (0.1% Formic acid) and flowrate of 0.2 µL/min. MS-mode scans were collected from 400 to 2,000 m/z with a resolution setting of 70,000 and target intensity of 3e6. A data dependent Top25 method was used to select precursors to fragment by HCD (Normalized Collision Energy = 30) at an MS/MS resolution of 17,500, target intensity at 1e5 and isolation window of 4.0 m/z.

The samples for the gas phase ion/ion reactions were prepared as follows: Prior to crosslinking reactions, α-Synuclein was buffer exchanged twice into fresh 50 mM ammonium acetate, pH 6.85 before electrospray ionization at a final concentration of 20 µM. The proton transfer reagent, PFO was electrosprayed at 1.25 mM in a 99/1 vol/vol mixture of methanol/ammonium hydroxide and the crosslinking reagents (1,2-BDSA, 1,3-BDSA and 1,5-NDSA) were first prepared at a concentration of 50mM in water and incubated with Amberlite cation exchange resin to facilitate ion exchange of Na+ and K+ and increase the relative concentration of doubly deprotonated form of the reagent. Following the ion exchange step, the stock solutions were diluted to a working concentration of 1mM using an 80/20 vol/vol mixture of acetonitrile/water. The remaining crosslinkers (Sulfo-EGS, BS3 and BS2G) were dissolved in acetonitrile at a final concentration of 1mM.

Ion/ion reactions were performed on the modified Synapt instrument (vide supra). The protein cations were introduced via pulled borosilicate tips while the anionic reagents were infused through the reference nanoflow sprayer at a flow rate of 1 µL/min. The external voltage control module was used to synchronize the source polarity (+1.0 kV and −1.0 kV) and ion injection times (1s each) to sequentially introduce the anions and cations into the instrument. α-Synuclein charge states and reagent ions (either deprotonated PFO or doubly deprotonated crosslinker) were isolated in the quadrupole and stored in the trap cell with a trap traveling wave height of zero volts to allow for gas phase ion/ion reactions of specific protein charge states to occur. The ion/ion

products were then separated by ion mobility (IM) using nitrogen as the mobility gas at a flow rate of 10 mL/min while the Trap, He and Transfer cell flow rates were set to 10, 10 and 5 mL/min, respectively. This lower pressure regime was used to maintain conditions in the trap cell conducive to stable ion/ion product formation, as previously published.[6] A ramping traveling wave velocity of 800 – 3000 m/s over a full IMS cycle and wave height of 40 V were used in the mobility cell. After IM separation, the ions were subjected to ECD fragmentation (using 3.5 eV electrons) in the ExD cell before mass analysis in the time-of-flight (TOF) mass spectrometer set to 'Resolution' mode. All reactions were performed in triplicate runs to ensure reproducibility.

Data Analysis. For the gas phase ion/ion reactions, the IM peaks of the 1x crosslinked adduct or the 2x proton transfer product (by PFO) were selected, and the m/z data extracted using MassLynx v4.2 (Waters Corp.). All data were smoothed with two-point Savitsky-Golay smoothing and centered and a lockmass correction (769.3741, 1040.5504, or 1513.5959 m/z corresponding to c6+, c202+ and y13+ fragments respectively) was applied. The processed data was exported as .mgf (Mascot Generic Format) files, and c and z fragments were annotated using LCMS spectator[8] or ExDViewer v4.1.32 (e-MSion),[9] using a mass error tolerance of 20 ppm.[10] Custom modifications were included at the N and C termini to identify the modified ECD fragments. For in-solution crosslinking, these corresponded to the covalent addition of crosslinkers: 96.0211 Da (BS2G, $C_5H_4O_2$), 138.0681 Da (BS3, $C_8H_{10}O_2$), 226.0478 Da (sulfo-EGS, $C_{10}H_{10}O_6$), 96.0439 Da (MDH, $C_3H_4N_4$), and 143.0908 (ADH, $C_6H_{10}N_4$). For gas-phase crosslinking via ion/ion reactions, these corresponded to 237.9606 Da (1,2-BDSA and 1,3-BDSA), 287.9762 Da (1,5-NDSA), 485.9886 Da (BS2G), 528.0356 Da (BS3) and 616.0153 Da (sulfo-EGS). The triplicate data were filtered to only include fragments observed in at least two out of three runs and manually verified before visualizing the sequence maps in ExDViewer or Prosight Lite.[11] Crosslinked peptides obtained after Glu-C digest were analyzed using default settings in pLink v2.3.11[12] (SYUA_HUMAN P37840 UniProt database, Glu-C up to 3 missed cleavages, 600 ≤ Peptide Mass

≤ 6000, 6 ≤ Peptide Length ≤ 60, Precursor and Fragment Tolerance ± 20 ppm, no fixed or variable modifications, Result Filter Tolerance ± 10 ppm, Separate FDR ≤ 5 % at PSM level).

Structure Modeling and Analysis. 10,000 αSN structures were generated by IDPConformerGenerator.[13] IDPConformerGenerator produces IDP conformers by sampling sequence fragments of an input protein sequence against a non-redundant, high-resolution crystallography PDB database,[14] retrieving ω (Cβ-N), ϕ (N-Cα), and ψ (Cα-β) torsion angles and secondary structures for residues within the sequence fragments. Backbone-only conformers are generated, computing Lennard-Jones potentials parameterized from the Amber14SB force field for selecting energetically favored conformations over disfavored ones with steric clashes. Side chains were added using a Monte Carlo approach in the MC-SCE algorithm.[15] All other settings were used as recommended. Structures generated from IDPConformerGenerator were filtered by interresidue distance; the distance between crosslinked Cα pairs identified by fragmentation of the intact αSN monomer was compared to the following distance: the sum of the linker length plus the side chain length (6.4 Å for lysine, 1.5 Å for the N-Cα distance on the N terminal residue, 4.5 Å for aspartic acid, and 6.0 Å for glutamic acid) with an additional “padding” of 10 Å, 4 Å longer than the prescribed “padding” distances for well-folded proteins[16] to account for additional dynamics in IDPs. Conformers that did not satisfy the restraints were filtered out.

CCS distributions were predicted directly from the NMR[17] and chemical crosslinking solution ensembles by the projection superposition approximation (PSA)[18] with nitrogen as a collision gas. Default parameters were used. Gas phase structural ensembles of αSN were calculated with the structure relaxation approximation (SRA)[19] using the NMR solution ensemble (vide supra) as starting structures. Briefly, after quick relaxation in solvent, the SRA assigns charges to titratable residues based on the input charge state by solvent accessible surface area (SASA) and geometry optimization by semi-empirical methods. Then, sequential gas phase molecular dynamics simulations are carried out ramping the temperature in steps of 100 K from 300 to 600 K back to 300 K, followed by 2 ns of MD simulations at 300 K with 200 conformers saved across

the trajectory. Finally, the PSA is used to calculate the CCS distributions from the saved conformers.

Distances for the SRA, solution crosslinking, and NMR ensembles, including the end-to-end distance (Ree), the radius of gyration (Rg), and the SASA were calculated in GROMACS.[20-21] The remaining conformers were clustered into six groups using the tool TTClust[22] with default settings. SRA calculations were performed at the high performance computing cluster at Florida State University, and all other structure prediction and analysis calculations were performed on either the Big Red 3 or Big Red 200 high performance computing clusters at Indiana University.

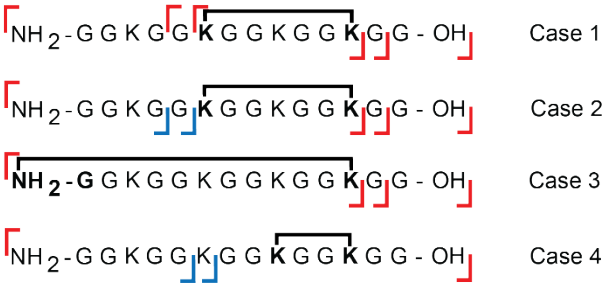

Supporting Scheme 1. Types of crosslinks and their associated fragmentation patterns. Red flags indicate the mass of the fragment plus crosslink, blue flags indicate the mass of an unmodified fragment, and X over a transparent flag indicates that in that case, those fragments specifically are not observed. Crosslinks are shown in black and crosslinked residues are bolded. Flags around the N and C-termini indicate that the precursor ion is crosslinked (or unmodified, in the case of the control).

Scheme 1 shows the different possibilities of fragmentation for a hypothetical peptide containing five reactive groups (the N-terminus, K3, K6, K9, and K12) and the resulting annotations of crosslinks that match the observed fragmentation patterns. Case 1 illustrates when a region of the sequence with at least two reactive amino acids is bracketed by modified N-terminal *z* ion(s) and C-terminal *c* ions(s) (z_9, z_{10}, c_{12}, and c_{13} in the hypothetical peptide). The reactive residues closest to the modified fragments (i.e., K6 and K12) are crosslinked in this case. Crosslinks between either of these two residues and K9 are less likely since fragments are observed in the control experiment but not Case 1. Fragmentation still occurs in this region but is not observed because the crosslink holds the two complementary fragments in this region,

“silencing” observed fragmentation between residues that are within two crosslinked residues in the primary sequence. Case 2 is crosslinked in the same place as Case 1, except the unmodified complementary ions of modified z_9 and z_{10} are observed instead. The presence of the complementary ions indicate that the modified fragments must exist; however, their intensities could be significantly reduced by some other crosslink such that they are not observed. Case 3 is simply a different version of Case 1, where the crosslink is localized between the N-terminus and K12. Since there are no modified *z*-ions N-terminal to the modified *c*-ions, the crosslink can best be explained as occurring at the N-terminus. Case 4 is simply the C-terminal version of Case 2, where the complementary ions of modified z_8 and no C-terminal *c* ions is best explained by crosslinking between K9 and the most C-terminal reactive site, K12.

Figures S3 and S5 show the fragments observed for the BS2G crosslinked and unmodified control versions, respectively, from ECD of αSN. The annotation of crosslinking assignments for this charge state is described below to show the application of the Scheme S1 crosslink types to our data. We will examine the +9 charge state. Figure S5 shows ECD fragmentation of the unmodified +9 ions, where sequence coverage between each reactive residue is achieved except for *z*-ions between the N-terminus and K6, and *c*-ions between K96/K97 and K102. Crosslinks are then assigned based on the ECD fragments from the singly BS2G-crosslinked +9 ions either not containing or containing the *m/z* increase due to the presence of BS2G (Figure S3). Crosslinks only spanning a few residues in the primary sequence are not structurally informative and are omitted.

The first modified fragment counting from the N-terminus is c_{17}, suggesting a Case 3 crosslink between the N-terminus and K12. The first modified fragment counting from the C-terminus is z_{105}, suggesting a Case 4 crosslink between K43 and either K96, K97, or K102. The end of the unmodified *c* ions following S42 also supports this assignment. The C-terminal lysine in this crosslink cannot be determined unambiguously due to the lack of *z* ions between these

residues. Each of these crosslinks is then validated against the unambiguously assigned crosslinks from denaturing LC-MS/MS of the Glu-C digested BS2G-linked protein (Table S3). N-terminus to K12 linking was found in both datasets. K43 to K96 but not K97 or K102 was found in the Glu-C digested dataset, suggesting that the second crosslink found from the +9 data is between K43 and K96.

If the fragmentation spectra are contaminated with fully unmodified protein, as they were for the acidic crosslinks, then the unmodified fragments cannot be used to assign linker locations, and only the modified fragments can be used for assignments.

Supporting Table 1. Agilent 6560 IM-QTOF Instrument Tuning Parameters (CCS Measurements).

Instrument Region	Instrumental Parameter	Experimental Value
Source	Gas Temp	310 °C
	Drying Gas	1.5 L/min
	Nebulizer	9 psi
	230	250 °C
	Sheath Gas Flow	5.5 L/min
	VCap	-3500 V
	Nozzle Voltage (Expt)	-1000 V
	Fragmentor	-300 V
	Oct 1 RF Vpp	750 V
High Pressure Funnel	High Pressure Funnel Delta	-110 V
	High Pressure Funnel RF	-180 V
Trapping Funnel	Trap Funnel Delta	-160 V
	Trap Funnel RF	-100 V
	Trap Funnel Exit	-10 V
	Entrance Grid Delta	-2 V
	Entrance Grid Low	-70 V
	Entrance Grid High	-72 V
	Trap Entrance	-69 V
	Trap Exit	-67 V
	Trap Fill Time	2000 µs
	Trap Release Time	250 µs
	Trap Exit Grid 1 Delta	-5 V
	Trap Exit Grid 1 Low	-64V
	Trap Exit Grid 1 High	-69 V
	Trap Exit Grid 2 Delta	-9 V
	Trap Exit Grid 2 Low	-63 V
	Trap Exit Grid 2 High	-72 V
Drift Tube	Drift Tube Entrance Voltage	Range -1700-1200 V
	Drift Tube Exit Voltage	-250 V
	Drift Tube Field Strength	-18.5 V/cm
Rear Funnel	Rear Funnel Entrance	-240
	Rear Funnel RF	-100
	Rear Funnel Exit	-43
	IM Hex Delta	-8
	IM Hex RF	-600
	IM Hex Entrance	-41

Supporting Table 2. Synapt G2-Si IM-QTOF Instrument Tuning Parameters (CCS Measurements).

Instrument Region	**Instrumental Parameter**	**Experimental Value**
Source	Capillary	1.0 kV
	Temperature	80 °C
Stepwave 1	Wave Velocity	300 m/s
	Wave Height	10 V
Stepwave 2	Wave Velocity	300 m/s
	Wave Height	0 V
IMS	Wave Velocity	300 m/s
	Wave Height	40 V
Transfer	Wave Velocity	169 m/s
	Wave Height	5 V
Triwave Trap	Wave Velocity	300 m/s
	Wave Height	1 V
Gas Controls	Trap	10 mL/min
	Helium Cell	200 mL/min
	IMS	50 mL/min
	Transfer	3 mL/min
Trap DC	Entrance	3
	Bias	40
	Trap DC	-10
	Exit	0
IMS DC	Entrance	12
	He Cell DC	20
	He Cell Exit	-12
	Bias	50
	Exit	20
Transfer DC	Entrance	20
	Exit	20

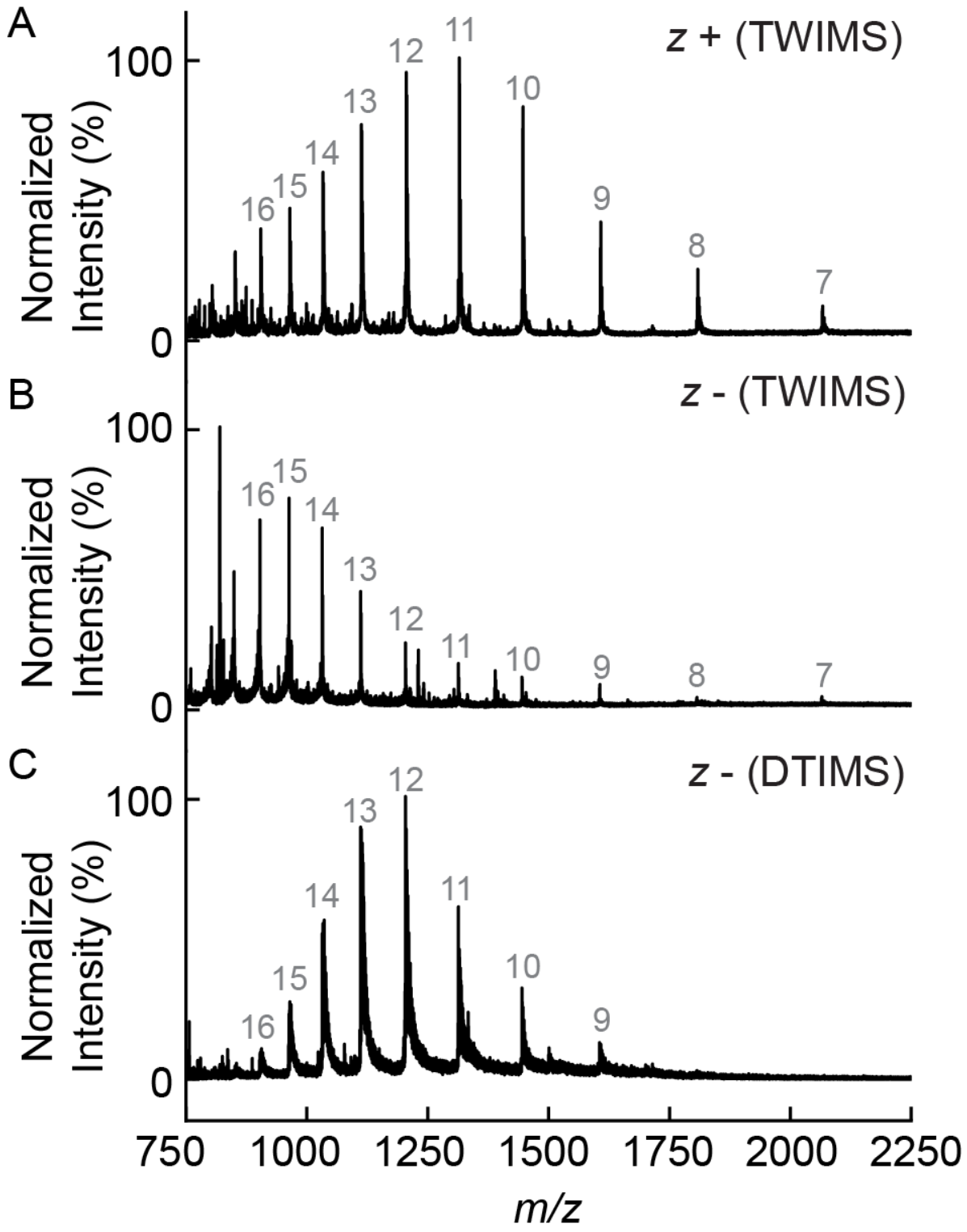

Figure S1. Charge state distributions (CSDs) for α-Synuclein observed using different electrospray polarity and ion mobility methods. CSDs observed using (A) positive and (B) negative

nano electrospray ionization (nESI) on Synapt G2Si. (C) CSD observed using negative ESI on Agilent 6560.

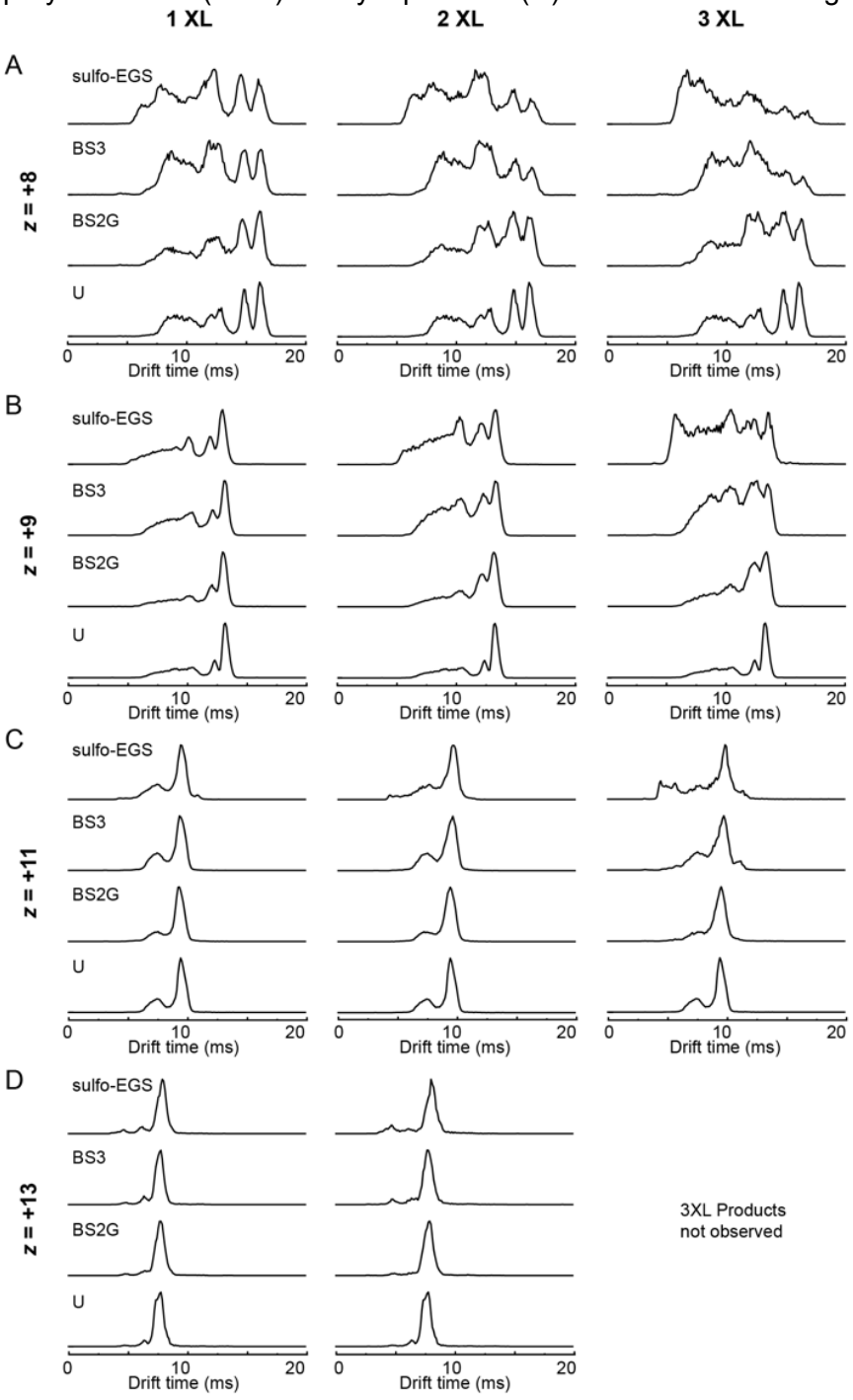

Figure S1. Arrival time distributions (ATDs) of αSN products crosslinked with BS2G, BS3 and sulfo-EGS. *ATDs were isolated for different charge states (z = +8, +9, +11 and +13). (A) – (D) ATD plots for individual charge states show the drift time profiles of multiply crosslinked products (1 to 3XL) compared to an unreacted sample (U) and only the 1XL products undergo minimal*

disruption in their ATDs.

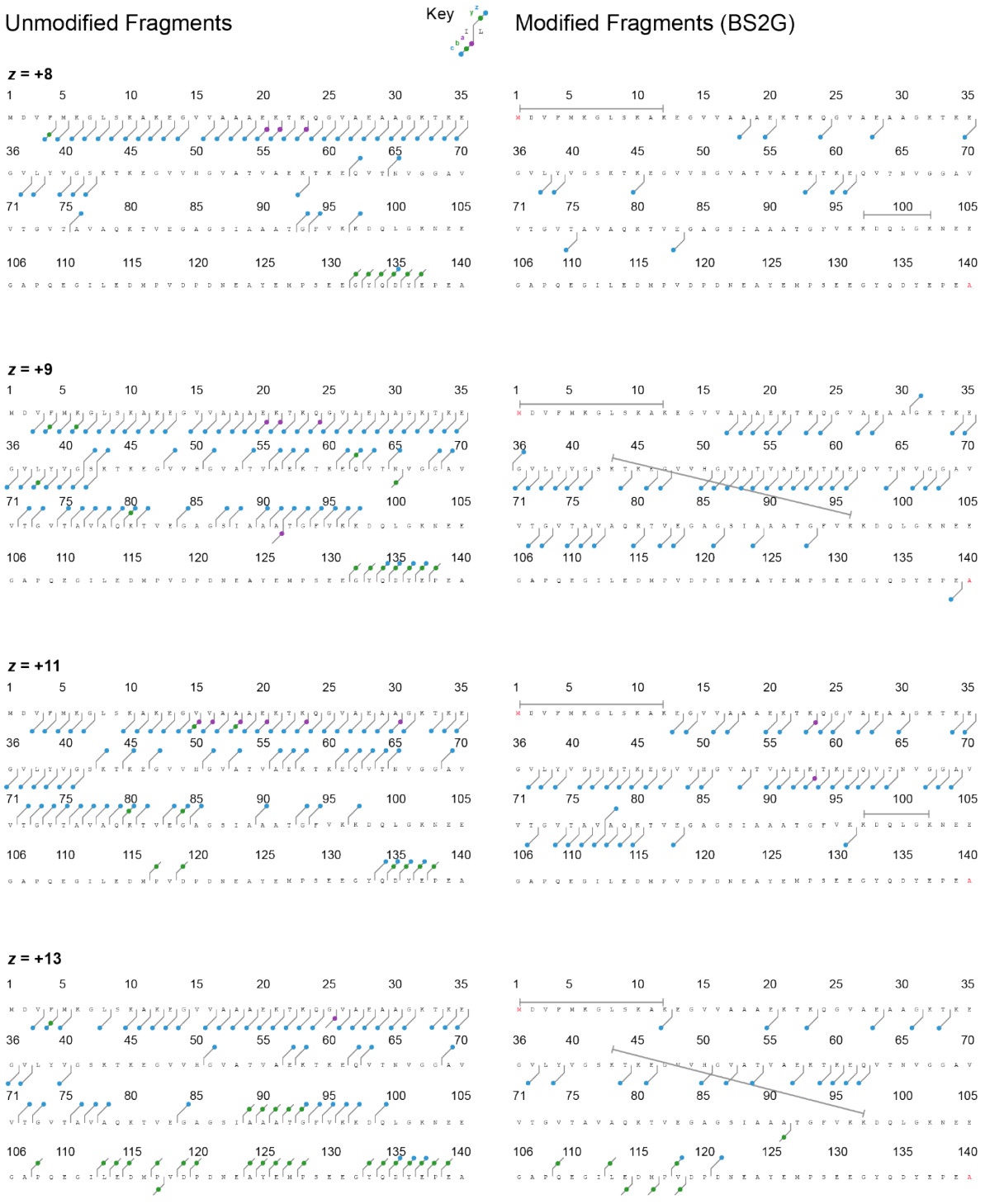

Figure S3. Sequence maps of BS2G crosslinked αSN (z = +8, +9, +11 and +13). *Unmodified fragments (left). Fragments with* covalent mass adduct formed by BS2G (right). Different ion types are displayed as follows: c and z (blue), b and y (green) and a (purple). Identified crosslinked residues are connected in gray.

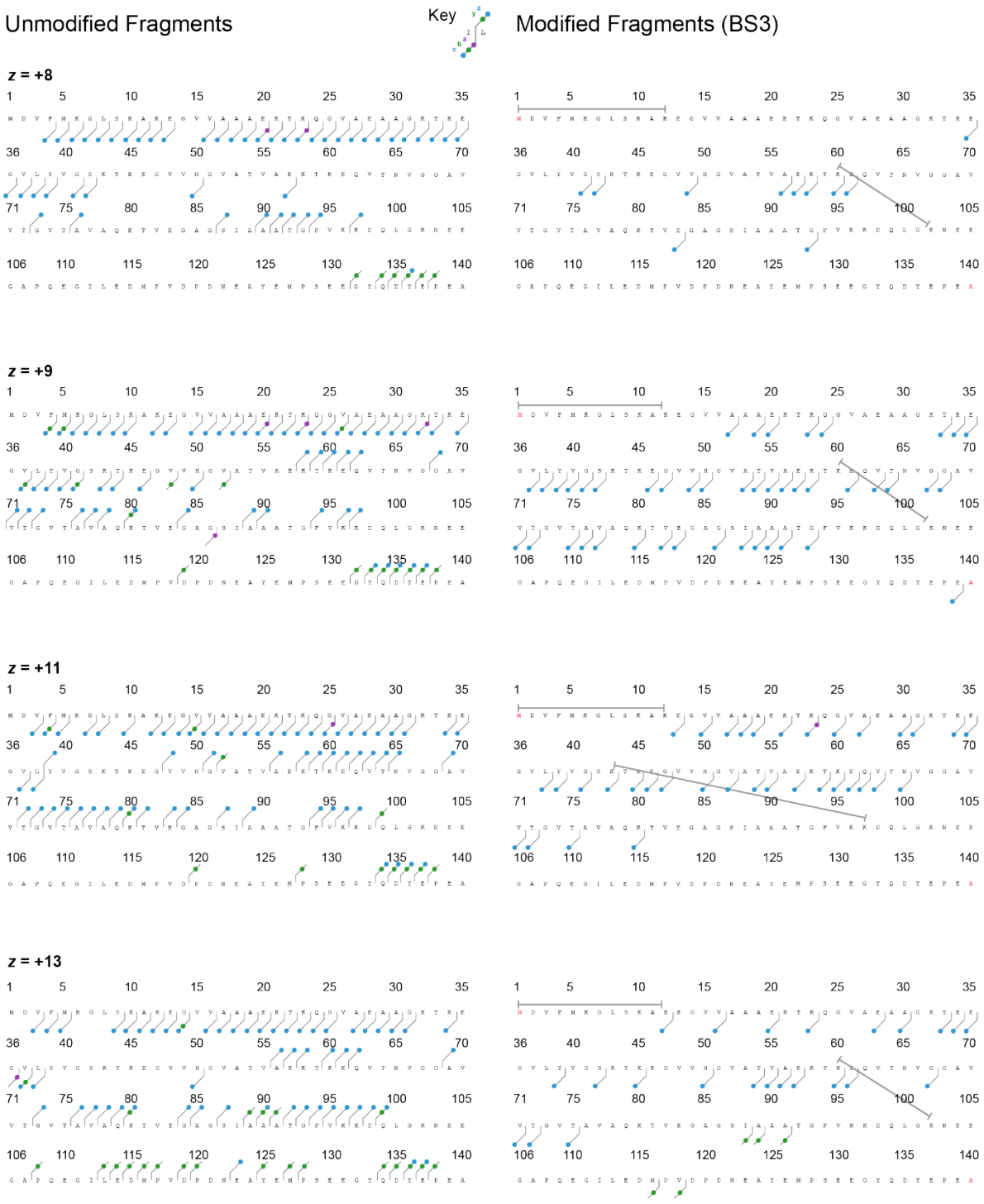

Figure S4. Sequence maps of BS3 crosslinked αSN (z = +8, +9, +11 and +13). *Unmodified fragments (left). Fragments with covalent mass adduct formed by BS3 (right).* Different ion types are displayed as follows: c and z (blue), b and y (green) and a (purple). Identified crosslinked residues are connected in gray.

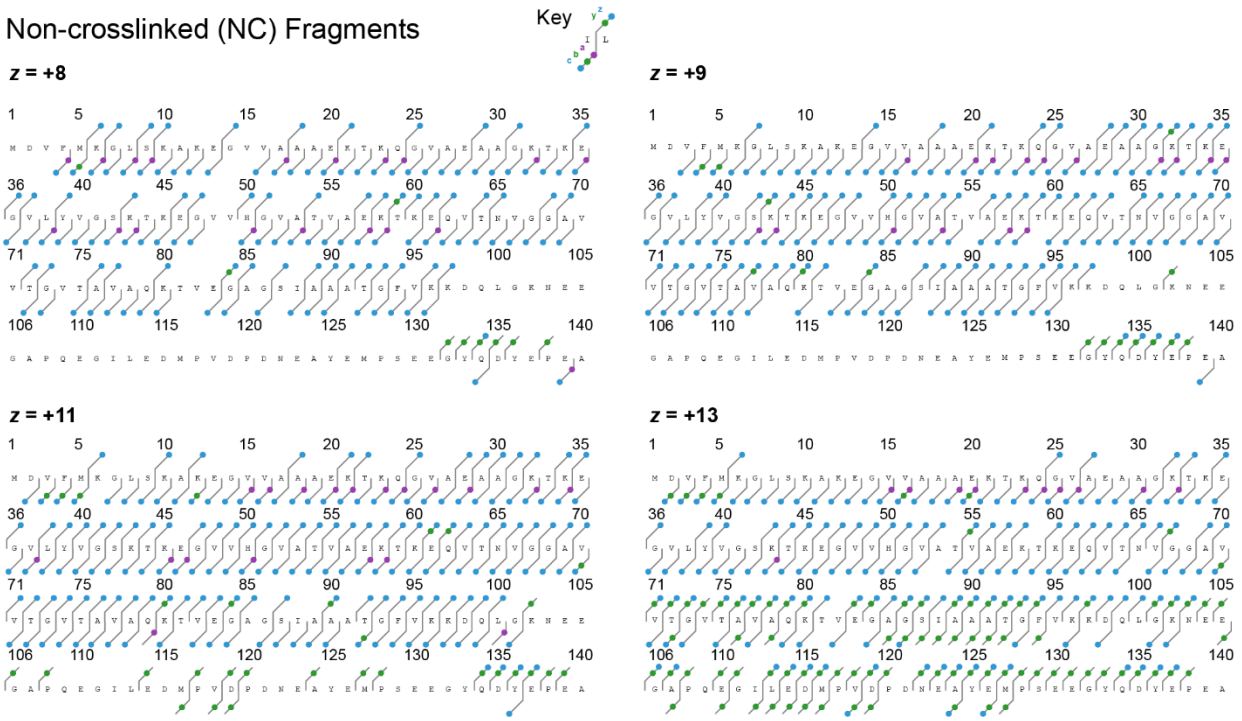

Figure S5. Sequence maps of non-crosslinked αSN (z = +8, +9, +11 and +13). *Non-crosslinked (NC) fragments are observed across the entire sequence, showing that fragmentation is efficient in the absence of crosslinking.*

Figure S6. Sequence maps of MDH crosslinked αSN (z = +8, +9, +11 and +13). *Unmodified fragments (left)*. *Fragments* containing the covalent mass adduct formed by MDH (right). Different ion types are displayed as follows: c and z (blue), b and y (green) and a (purple). Identified crosslinked residues are connected in gray.

Figure S7. Sequence maps of ADH crosslinked αSN (z = +8, +9, +11 and +13). *Unmodified fragments (left). Fragments containing the covalent mass adduct formed by ADH (right). Different ion types are displayed as follows: c and z (blue), b and y (green) and a (purple). Identified crosslinked residues are connected in gray.*

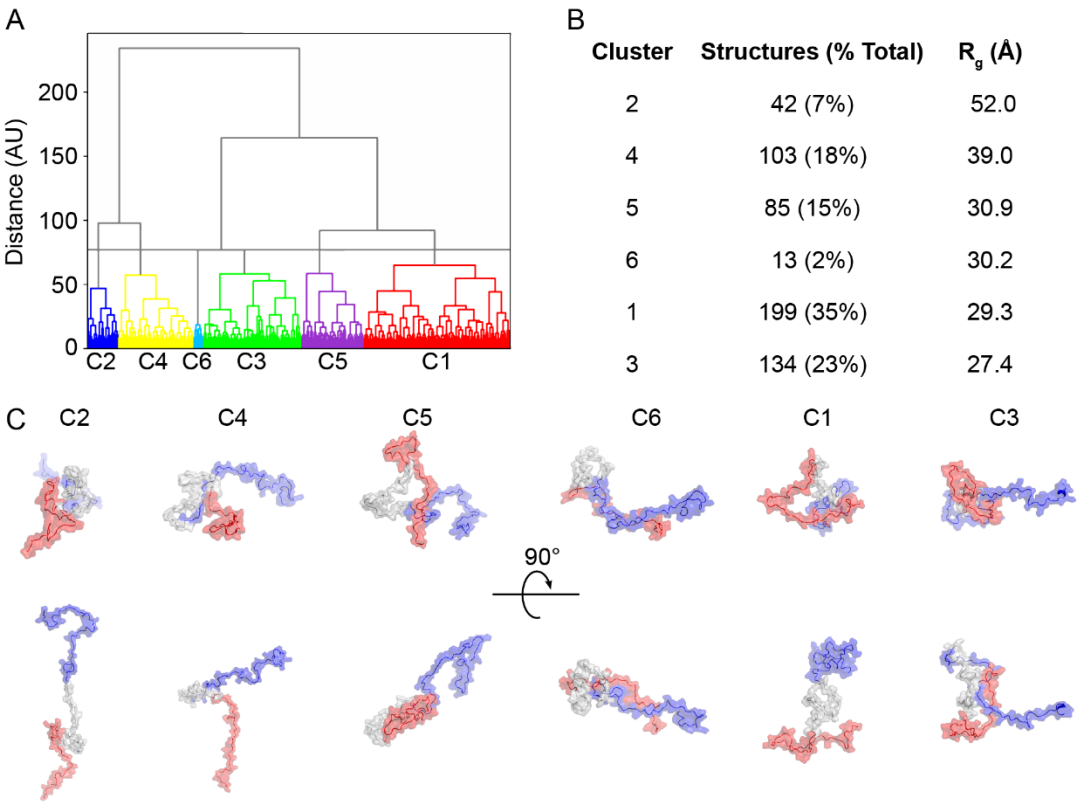

Figure S8. Summary of clustered NMR structural ensemble (n = 576, C1 - C6). *(A) Cluster dendrogram showing distribution of conformational space into specific clusters. (B) Table summarizing the number of structures per cluster in order of decreasing* R_g. (C) Representative structures for each cluster, rotated 90º along the x-axis and the αSN structure is colored as blue (N-terminal region, residues 1 – 60), gray (Nonamyloid-β component, residues 61 – 95) and red (C-terminal tail, residues 96 – 140).

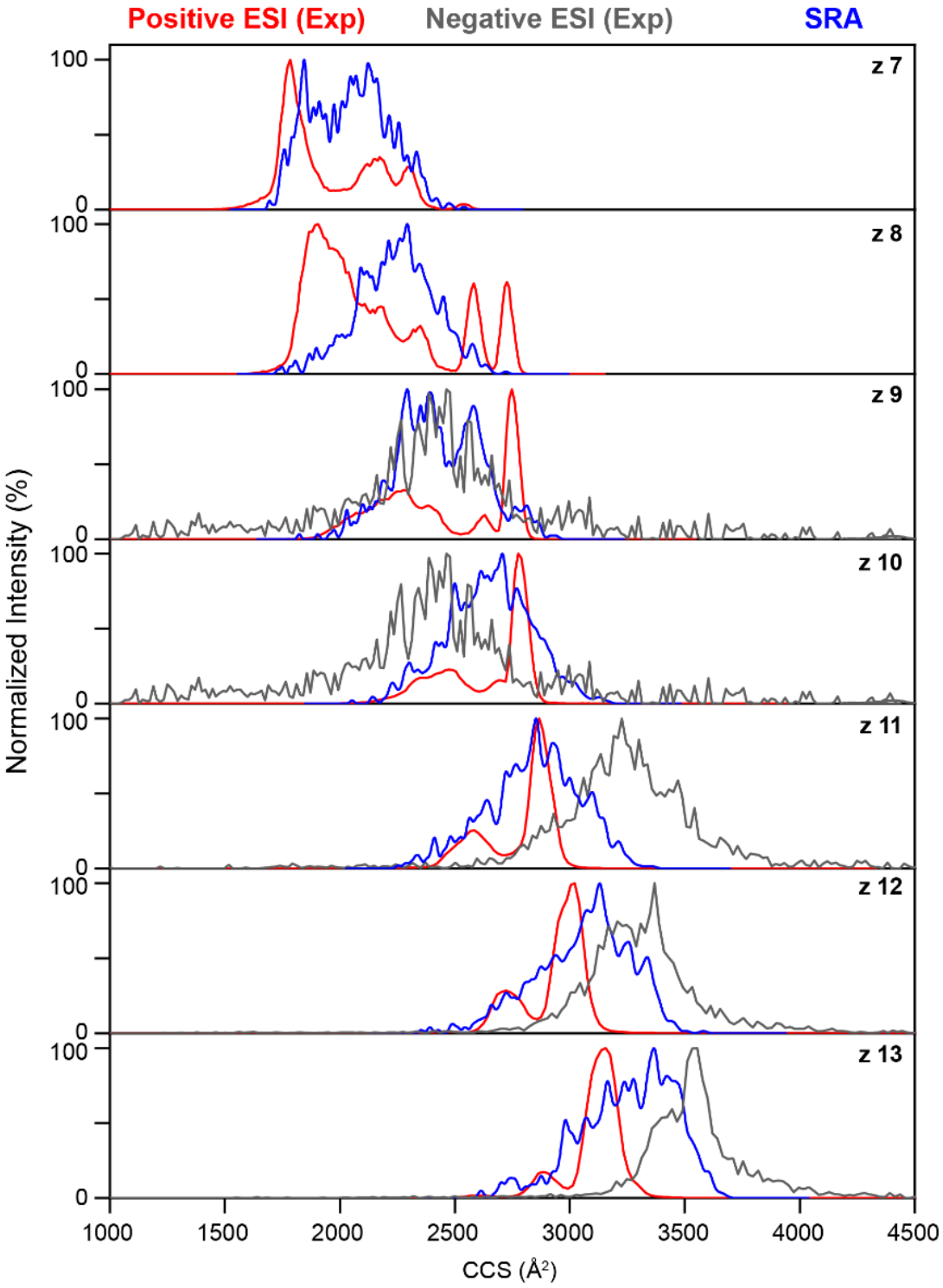

Figure S9. Normalized intensity of ATDs plotted against CCS measured experimentally in positive (z +) and negative (z -) ESI as well as CCS of gas phase ensemble modeled using structure relaxation approximation (SRA). *CCS was measured in positive and negative ESI using TWIMS (red, z* = +7 to +13) and DTIMS (gray, *z* = -9 to -13) respectively. CCS was also calculated from gas-phase structures modeled using SRA (blue, *z* = +7 to +13).

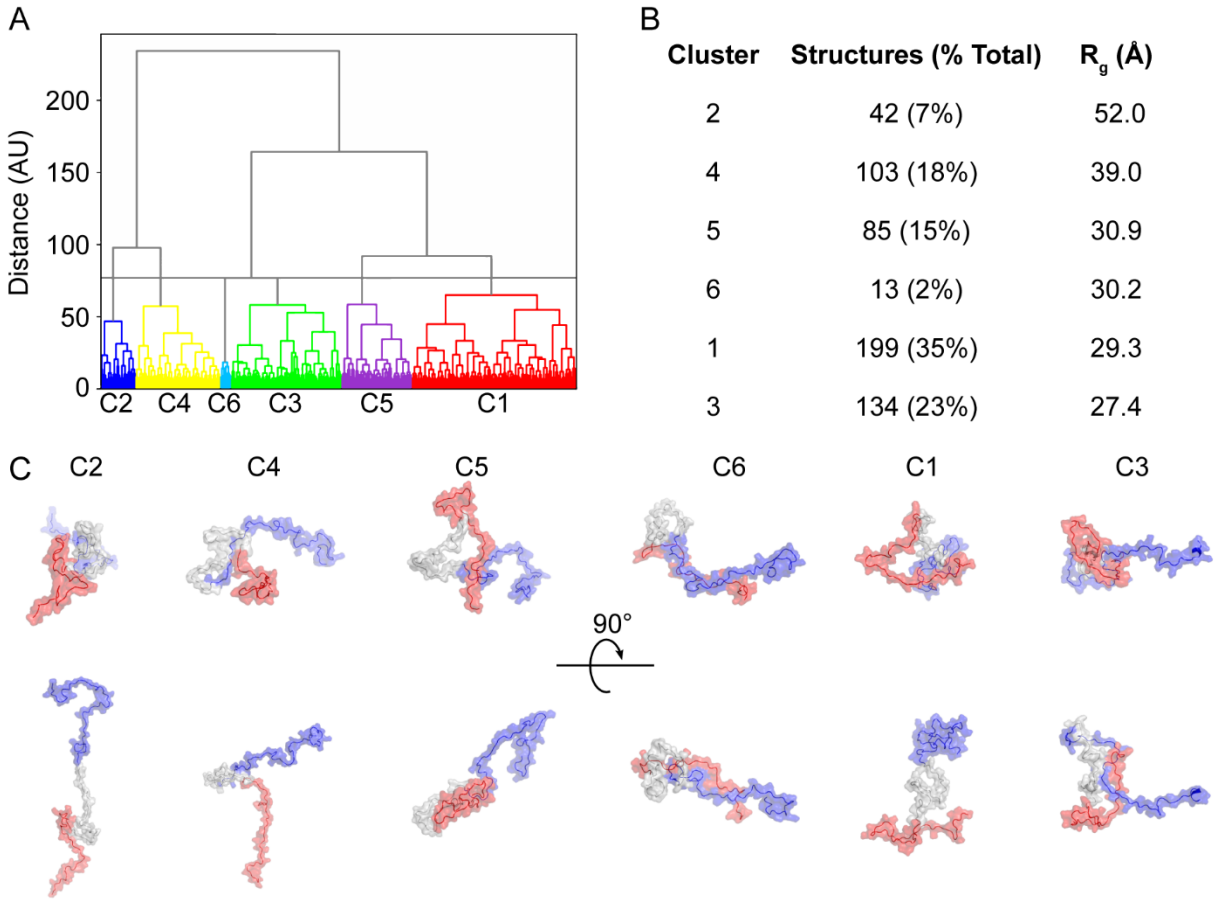

Figure S10. Clustered PRE NMR (n = 576) structural ensemble. *(A) The cluster dendrogram shows the distribution of conformational space into specific clusters for PRE NMR. (B) Representative structures for each cluster,* rotated 90º along the x-axis and the αSN structure is colored as blue (N-terminal region, residues 1 – 60), gray (Nonamyloid-β component, residues 61 – 95) and red (C-terminal tail, residues 96 – 140).

Supporting Table 3. Summary of Identified Crosslinking Sites Using a Bottom-up Approach and Glu-C Digest Step.

Reagent	Crosslinked peptides observed ≥ 2 out of 3 replicates				
BS2G	N-term – K6	K6 – K10	K21 – K23	K34 – K43	K96 – K102
	N-term – K12	K6 – K43	K21 – K45		
	N-term – K43	K6 – K80	K21 – K58	K43 – K58	K97 – K102
	N-term – K58			K43 – K60	
	N-term – K80		K23 – K102	K43 – K80	
	N-term – K96		K23 – K43	K43 – K96	
			K23 – K45		
				K45 – K96	
BS3	N-term – K12	K6 – K96	K10 – K80	K43 – K45	K60 – K102
	N-term – K80			K43 – K80	
			K12 – K80	K43 – K96	K96 – K102
					K96 – K97
					K97 – K102

Supporting Table 4. Summary of Gas-phase Ion/Ion Products Formed from αSN Precursors, z = +11 and +13.

Reagent Anion	**m/z product (*z* = +11 → +9)**	**m/z after ECD (*z* = +8)**
PFO (799.0 m/z)	1607.8	1808.8
1,2-BDSA (118.0 m/z)	1634.2	1838.5
1,3-BDSA (118.0 m/z)	1634.2	1838.5
1,5-NDSA (143.0 m/z)	1639.8	1844.8
BS2G (242.0 m/z)	1661.8	1869.5
BS3 (263.0 m/z)	1666.5	1874.8
Sulfo-EGS (307.0 m/z)	1676.2	1885.8
Reagent	**m/z product (*z* = +13 → +11)**	**m/z after ECD (*z* = +10)**
PFO (799.0 m/z)	1315.5	1447.2
1,2-BDSA (118.0 m/z)	1337.3	1471.1
1,3-BDSA (118.0 m/z)	1337.3	1471. 1
1,5-NDSA (143.0 m/z)	1341.8	1476.0
BS2G (242.0 m/z)	1359.8	1495.8
BS3 (263.0 m/z)	1363.7	1500.0
Sulfo-EGS (307.0 m/z)	1371.7	1508.8

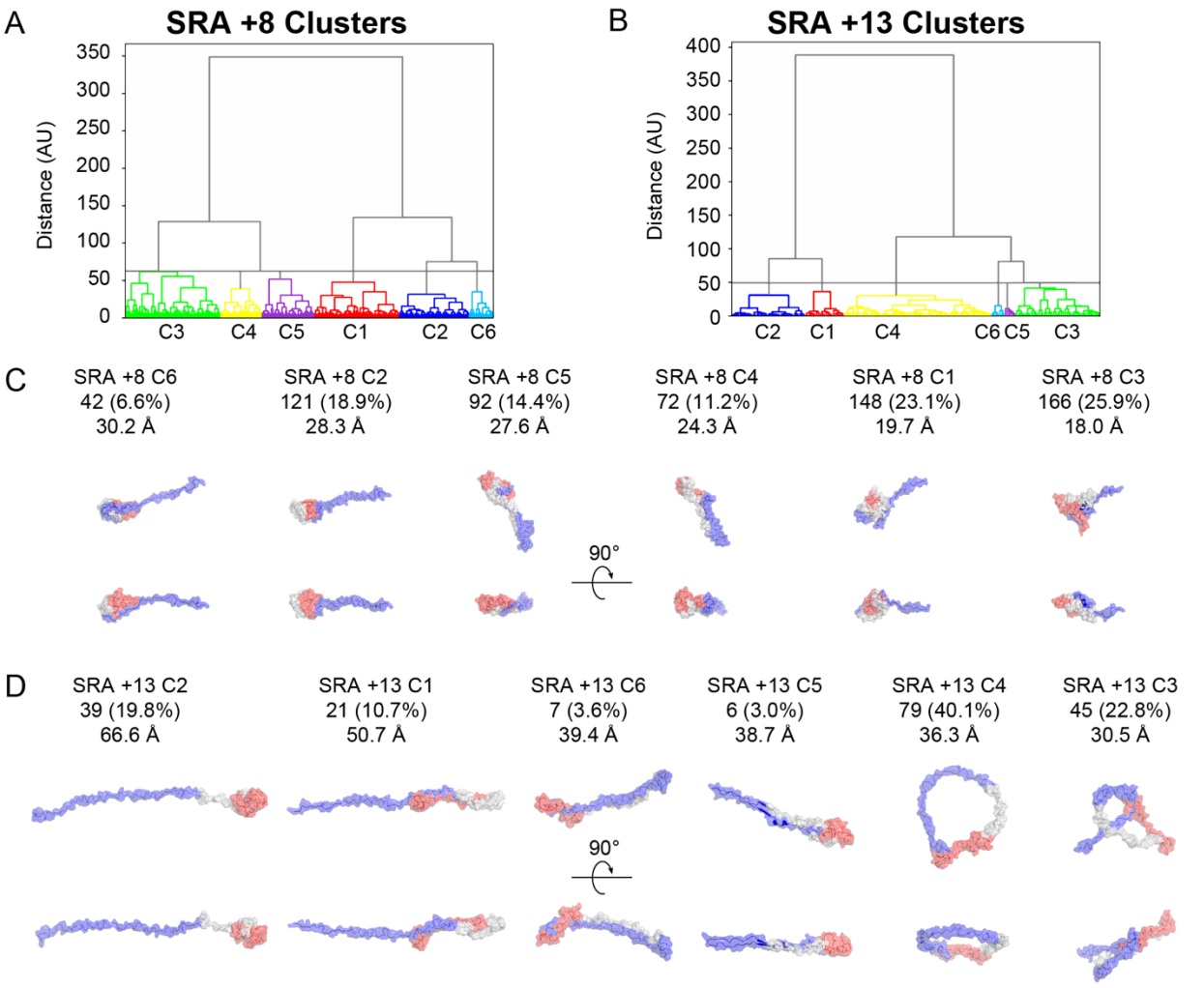

Figure S11. Clustered SRA +8 (n = 641) and +13 (n = 197) structural ensembles. *Cluster dendrograms show distribution of conformational space into specific clusters for SRA (A) +8 and (B) +13 datasets, respectively. Representative conformers for each cluster, rotated 90º along the x-axis and the αSN structure is colored as blue (N-terminal region, residues 1 – 60), gray (Nonamyloid-β component, residues 61 – 95) and red (C-terminal tail, residues 96 – 140) for SRA (C) +8 and (D) +13 datasets, respectively.*

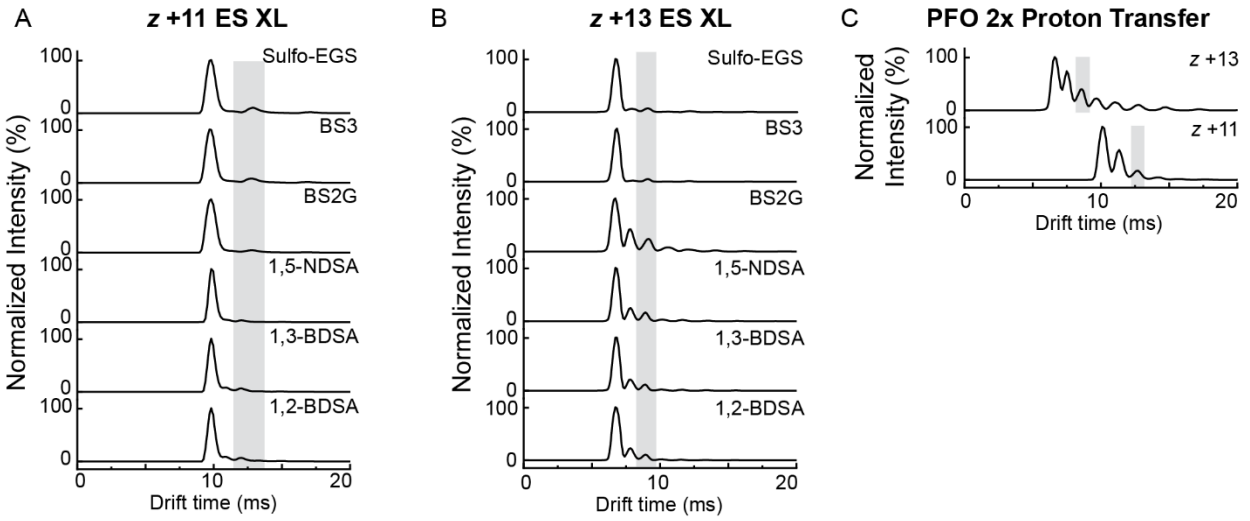

Figure S12. Arrival time distributions (ATDs) for αSN z = +11 and +13 and gas-phase ion/ion reactions. *Reactions were performed with* (A) electrostatic crosslinkers (ES XL, *z* = -2: 1,2-BDSA, 1,3-BDSA, 1,5-NDSA, BS2G, BS3 and sulfo-EGS) and (B) proton transfer reagent (PFO, *z* = -1), with IM peaks highlighted in gray corresponding to the 1x ES XL and 2x proton transfer products, which were further analyzed by ECD fragmentation.

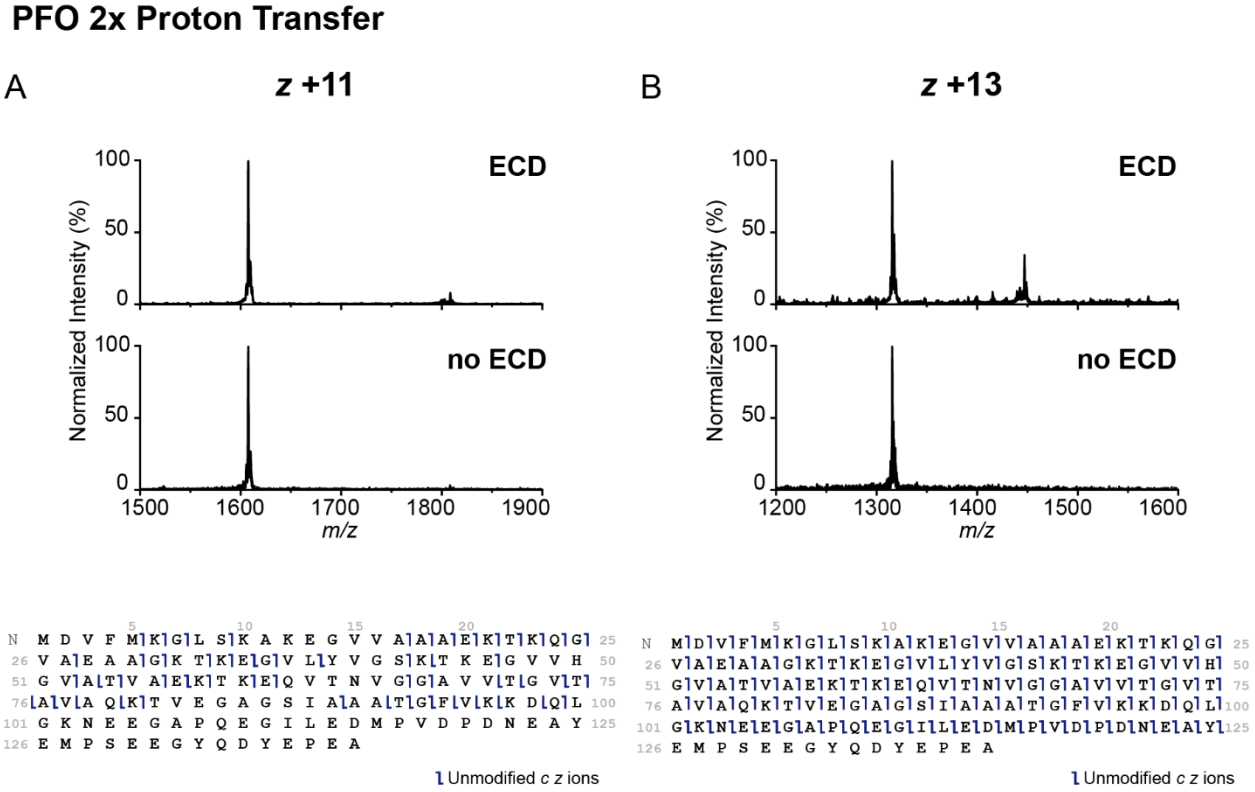

Figure S13. Summary of ECD data acquired for 2x proton transfer products formed using αSN z = +11 and +13. *Mass spectra (MS) showing 2x proton transfer product with αSN precursor (A) +11 and (B) +13, with and without ECD fragmentation and fragmentation maps showing sequence coverage by ECD. ECD is less efficient with lower charge state z* (+11 → +9) product compared to (+13 → +11), resulting from 2x proton transfer reactions with *z* +11 and +13 precursors respectively.

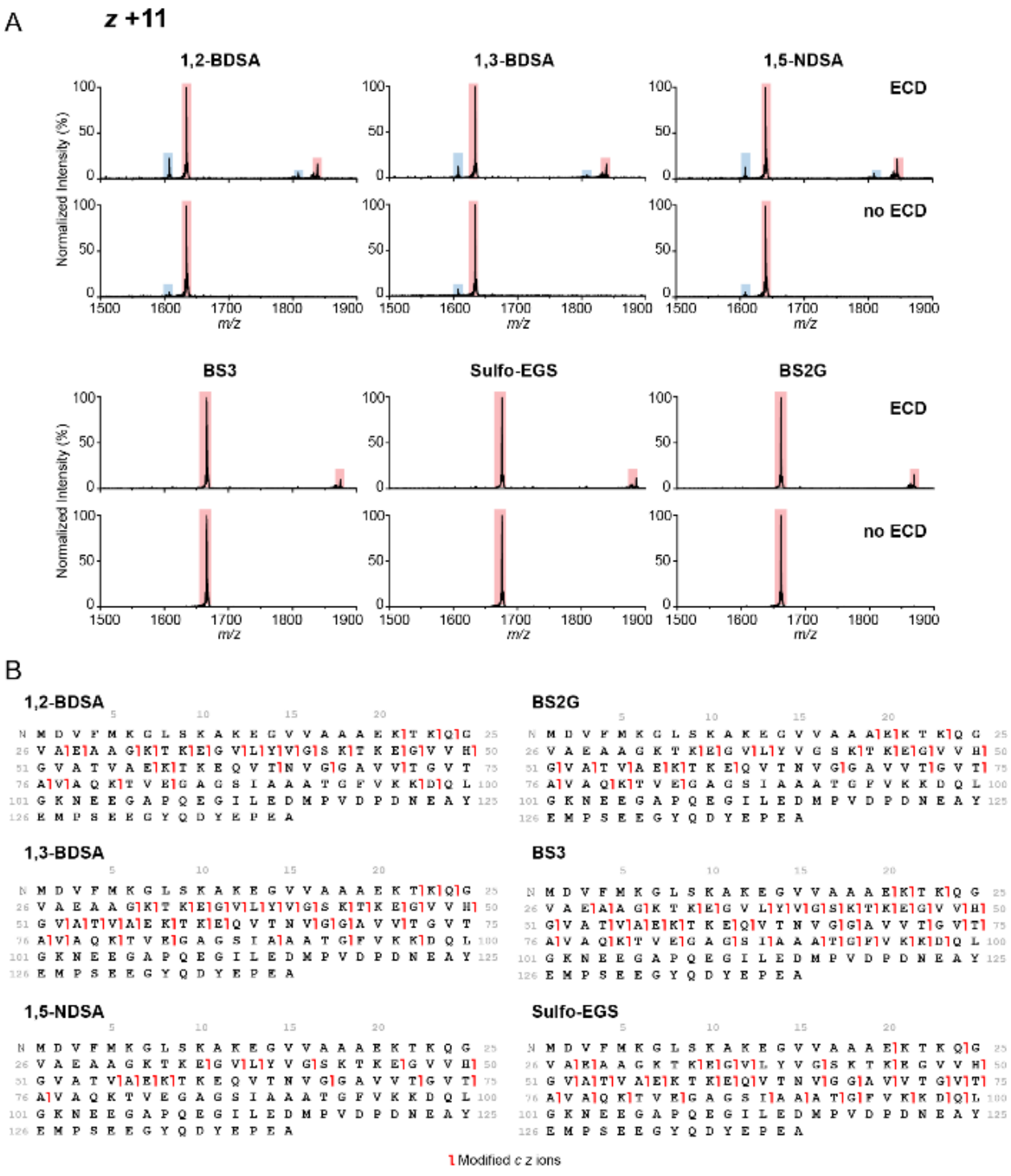

Figure S14. Summary of ECD data acquired for 1x electrostatic crosslinked (ES XL) products formed using αSN precursor, z = +11. *(A) Mass spectra (MS) showing 1x ES XL product with αSN +11 with and without ECD fragmentation, where 1x ES XL and 2x proton transfer (side product) peaks are highlighted in red and blue respectively. (B) Fragmentation maps showing sequence coverage by ECD and fragmentation patterns are used to assign crosslinked sites.*

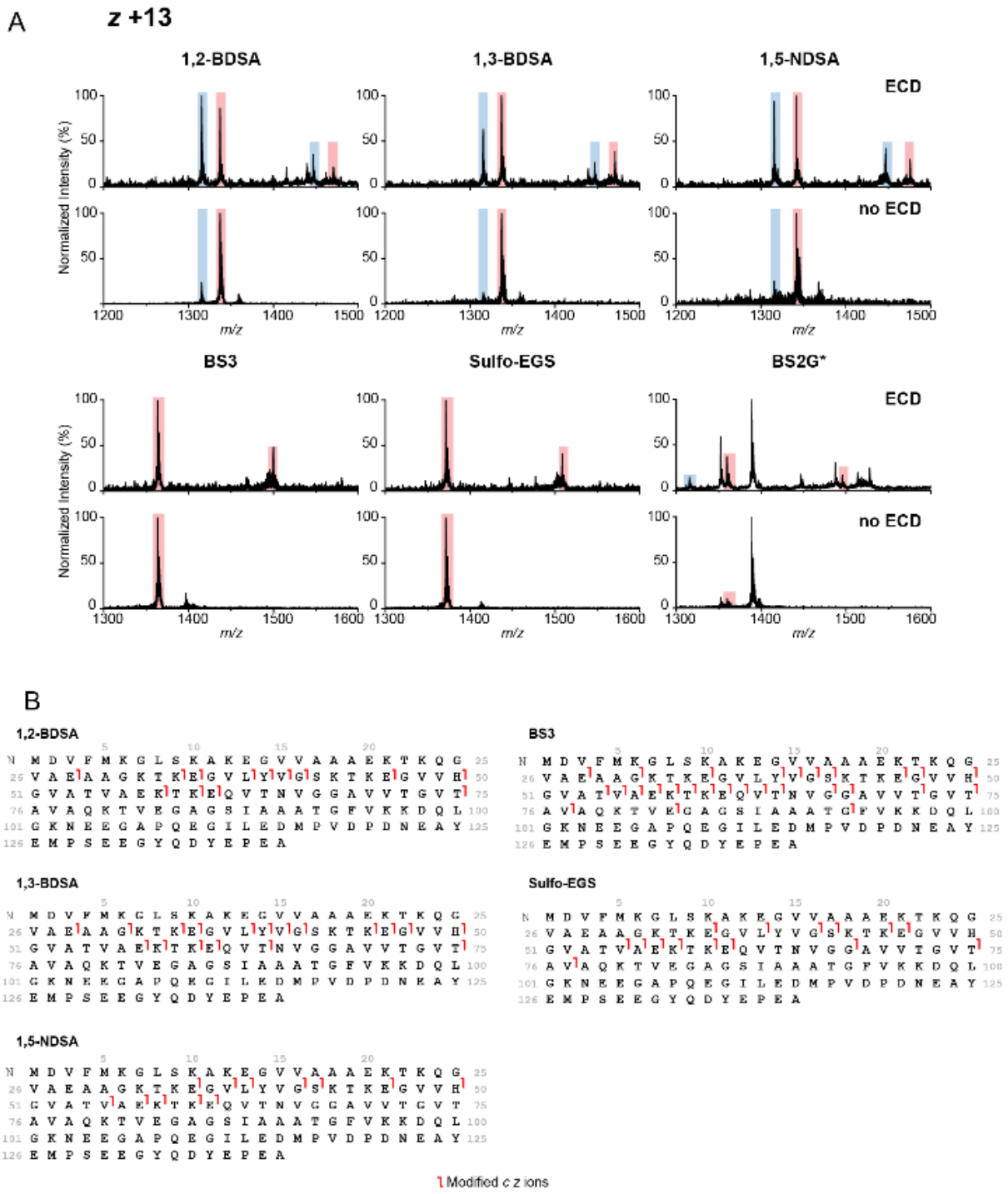

Figure S15. Summary of ECD data acquired for 1x electrostatic crosslinked (ES XL) products formed using αSN precursor, z = +13. *(A) Mass spectra (MS) showing 1x ES XL product with αSN +13 with and without ECD fragmentation, where 1x ES XL and 2x proton transfer (side product) peaks are highlighted in red and blue respectively. (B) Fragmentation maps showing sequence coverage by ECD and fragmentation patterns are used to assign crosslinked sites. BS2G was denoted with a * since 1x ES XL product was not the major product resulting from gas phase ion/ion crosslinking reaction and ECD fragments could not be analyzed unambiguously to assign crosslinked sites, thus was omitted in (B).*

Supporting Table 5. Summary of Identified Crosslinking Sites with αSN Precursors, z = +11 and +13.

Reagent	*z* +11	*z* +13
1,2-BDSA	N-term – K21	N-term – K21
1,3-BDSA		
1,5-NDSA	N-term – K34	N-term – K34
BS2G	N-term – K12	Not applicable
BS3		N-term – K21
Sulfo-EGS		N-term – K34

References

(1) Powers, A. E.; Patel, D. S., Expression and Purification of Untagged α-Synuclein. *Methods Mol Biol.* **2019,** *1948*, 261-269.
(2) Leitner, A.; Joachimiak, L. A.; Unverdorben, P.; Walzthoeni, T.; Frydman, J.; Förster, F.; Aebersold, R., Chemical cross-linking/mass spectrometry targeting acidic residues in proteins and protein complexes. *Proceedings of the National Academy of Sciences.* **2014,** *111*, 9455-9460.
(3) Fioramonte, M.; de Jesus, H. C. R.; Ferrari, A. J. R.; Lima, D. B.; Drekener, R. L.; Correia, C. R. D.; Oliveira, L. G.; Neves-Ferreira, A. G. d. C.; Carvalho, P. C.; Gozzo, F. C., XPlex: An Effective, Multiplex Cross-Linking Chemistry for Acidic Residues. *Anal. Chem.* **2018,** *90*, 6043-6050.
(4) Bush, M. F.; Hall, Z.; Giles, K.; Hoyes, J.; Robinson, C. V.; Ruotolo, B. T., Collision cross sections of proteins and their complexes: a calibration framework and database for gas-phase structural biology. *Anal. Chem.* **2010,** *82*, 9557-65.
(5) Webb, I. K.; Morrison, L. J.; Brown, J., Dueling electrospray implemented on a traveling-wave ion mobility/time-of-flight mass spectrometer: Towards a gas-phase workbench for structural biology. *Int J Mass Spectrom.* **2019,** *444*, 116177-116185.
(6) Carvalho, V. V.; See Kit, M. C.; Webb, I. K., Ion Mobility and Gas-Phase Covalent Labeling Study of the Structure and Reactivity of Gaseous Ubiquitin Ions Electrosprayed from Aqueous and Denaturing Solutions. *J Am Soc Mass Spectrom.* **2020,** *31*, 1037-1046.
(7) Williams, J. P.; Morrison, L. J.; Brown, J. M.; Beckman, J. S.; Voinov, V. G.; Lermyte, F., Top-Down Characterization of Denatured Proteins and Native Protein Complexes Using Electron Capture Dissociation Implemented within a Modified Ion Mobility-Mass Spectrometer. *Anal. Chem.* **2020,** *92*, 3674-3681.
(8) Park, J.; Piehowski, P. D.; Wilkins, C.; Zhou, M.; Mendoza, J.; Fujimoto, G. M.; Gibbons, B. C.; Shaw, J. B.; Shen, Y.; Shukla, A. K.; Moore, R. J.; Liu, T.; Petyuk, V. A.; Tolić, N.; Paša-Tolić, L.; Smith, R. D.; Payne, S. H.; Kim, S., Informed-Proteomics: open-source software package for top-down proteomics. *Nature Methods.* **2017,** *14*, 909-914.
(9) Beckman, J. S.; Voinov, V. G.; Hare, M.; Sturgeon, D.; Vasil'ev, Y.; Oppenheimer, D.; Shaw, J. B.; Wu, S.; Glaskin, R.; Klein, C.; Schwarzer, C.; Stafford, G., Improved Protein and PTM Characterization with a Practical Electron-Based Fragmentation on Q-TOF Instruments. *J Am Soc Mass Spectrom.* **2021,** *32*, 2081-2091.
(10) Donnelly, D. P.; Rawlins, C. M.; DeHart, C. J.; Fornelli, L.; Schachner, L. F.; Lin, Z.; Lippens, J. L.; Aluri, K. C.; Sarin, R.; Chen, B.; Lantz, C.; Jung, W.; Johnson, K. R.; Koller, A.; Wolff, J. J.; Campuzano, I. D. G.; Auclair, J. R.; Ivanov, A. R.; Whitelegge, J. P.; Paša-Tolić, L.; Chamot-Rooke, J.; Danis, P. O.; Smith, L. M.; Tsybin, Y. O.; Loo, J. A.; Ge, Y.; Kelleher, N. L.; Agar, J. N., Best practices and benchmarks for intact protein analysis for top-down mass spectrometry. *Nature Methods.* **2019,** *16*, 587-594.
(11) Fellers, R. T.; Greer, J. B.; Early, B. P.; Yu, X.; LeDuc, R. D.; Kelleher, N. L.; Thomas, P. M., ProSight Lite: graphical software to analyze top-down mass spectrometry data. *Proteomics.* **2015,** *15*, 1235-8.
(12) Chen, Z.-L.; Meng, J.-M.; Cao, Y.; Yin, J.-L.; Fang, R.-Q.; Fan, S.-B.; Liu, C.; Zeng, W.-F.; Ding, Y.-H.; Tan, D., A high-speed search engine pLink 2 with systematic evaluation for proteome-scale identification of cross-linked peptides. *Nature communications.* **2019,** *10*, 3404.
(13) Teixeira, J. M. C.; Liu, Z. H.; Namini, A.; Li, J.; Vernon, R. M.; Krzeminski, M.; Shamandy, A. A.; Zhang, O.; Haghighatlari, M.; Yu, L.; Head-Gordon, T.; Forman-Kay, J. D., IDPConformerGenerator: A Flexible Software Suite for Sampling the Conformational Space of Disordered Protein States. *J. Phys. Chem. A.* **2022,** *126*, 5985-6003.
(14) Wang, G.; Dunbrack, R. L., Jr., PISCES: a protein sequence culling server. *Bioinformatics.* **2003,** *19*, 1589-91.
(15) Bhowmick, A.; Head-Gordon, T., A monte carlo method for generating side chain structural ensembles. *Structure.* **2015,** *23*, 44-55.
(16) Merkley, E. D.; Rysavy, S.; Kahraman, A.; Hafen, R. P.; Daggett, V.; Adkins, J. N., Distance restraints from crosslinking mass spectrometry: mining a molecular dynamics simulation database to evaluate lysine-lysine distances. *Protein Sci.* **2014,** *23*, 747-59.
(17) Allison, J. R.; Varnai, P.; Dobson, C. M.; Vendruscolo, M., Determination of the Free Energy Landscape of α-Synuclein Using Spin Label Nuclear Magnetic Resonance Measurements. *J. Am. Chem. Soc.* **2009,** *131*, 18314-18326.
(18) Bleiholder, C.; Johnson, N. R.; Contreras, S.; Wyttenbach, T.; Bowers, M. T., Molecular Structures and Ion Mobility Cross Sections: Analysis of the Effects of He and N2 Buffer Gas. *Anal. Chem.* **2015,** *87*, 7196-7203.
(19) Bleiholder, C.; Liu, F. C., Structure Relaxation Approximation (SRA) for Elucidation of Protein Structures from Ion Mobility Measurements. *J. Phys. Chem. B.* **2019,** *123*, 2756-2769.

(20) Abraham, M. J.; Murtola, T.; Schulz, R.; Páll, S.; Smith, J. C.; Hess, B.; Lindahl, E., GROMACS: High performance molecular simulations through multi-level parallelism from laptops to supercomputers. *SoftwareX.* **2015,** *1-2*, 19-25.
(21) Páll, S.; Zhmurov, A.; Bauer, P.; Abraham, M.; Lundborg, M.; Gray, A.; Hess, B.; Lindahl, E., Heterogeneous parallelization and acceleration of molecular dynamics simulations in GROMACS. *J. Chem. Phys.* **2020,** *153*, 134110.
(22) Tubiana, T.; Carvaillo, J. C.; Boulard, Y.; Bressanelli, S., TTClust: A Versatile Molecular Simulation Trajectory Clustering Program with Graphical Summaries. *J Chem Inf Model.* **2018,** *58*, 2178-2182.